Organic & Biomolecular Chemistry

Dynamic Article Links

Cite this: *Org. Biomol. Chem.*, 2011, **9**, 5737

www.rsc.org/obc

PAPER

Surface active benzodiazepine-bromo-alkyl conjugate for potential $GABA_A$-receptor purification†

A. V. Turina,[a] G. J. Quinteros,[b] B. Caruso,[a] E. L. Moyano[b] and M. A. Perillo*[a]

Received 8th February 2011, Accepted 10th May 2011
DOI: 10.1039/c1ob05210a

A conjugable analogue of the benzodiazepine 5-(2-hydroxyphenyl)-7-nitro-benzo[*e*][1,4]diazepin-2(*3H*)-one containing a bromide C_{12}-aliphatic chain (BDC) at nitrogen N1 was synthesized. One-pot preparation of this benzodiazepine derivative was achieved using microwave irradiation giving 49% yield of the desired product. BDC inhibited FNZ binding to $GABA_A$-R with an inhibition binding constant $K_i = 0.89$ μM and expanded a model membrane packed up to 35 mN m^{-1} when penetrating in it from the aqueous phase. BDC exhibited surface activity, with a collapse pressure $\pi = 9.8$ mN m^{-1} and minimal molecular area $A_{min} = 52$ Å^2/molecule at the closest molecular packing, resulted fully and non-ideally mixed with a phospholipid in a monolayer up to a molar fraction $x \cong 0.1$. A geometrical–thermodynamic analysis along the π–A phase diagram predicted that at low x_{BDC} (<0.1) and at all π, including the equilibrium surface pressures of bilayers, dpPC–BDC mixtures dispersed in water were compatible with the formation of planar-like structures. These findings suggest that, in a potential surface grafted BDC, this compound could be stabilize though London-type interactions within a phospholipidic coating layer and/or through halogen bonding with an electron-donor surface *via* its terminal bromine atom while $GABA_A$-R might be recognized through the CNZ moiety.

1. Introduction

Purification of membrane bound proteins has always been a difficult challenge. It is a necessary step prior to many basic and applied studies. As an example, sometimes the isolation of proteins in a pure state may be required for their reconstitution in a model membrane. This would allow the evaluation – under controlled conditions – of the modulation induced by environmental properties such as composition, curvature, molecular packing, etc, on the conformation–activity relationship of an intrinsic membrane protein.[1–5] Protein purification is also required for the development of sensors or coated nanoparticles based on surface-grafted proteins through non-covalent immobilization which would be of major interest in bioanalytical sciences associated with the development of "lab-on-chips" systems.[6]

The integral membrane receptor $GABA_A$ ($GABA_A$-R) is a pentameric protein that acts as a ligand-gated chloride channel and is the site of action of a variety of pharmacologically important drugs including benzodiazepines.[7] $GABA_A$-R has been previously purified by ligand affinity chromatography[8] as well as by means of immunochemical techniques.[9] The development of a new purification method as a succedaneum of traditional inmunoprecipitation procedures to avoid the requirement of monoclonal antibodies against specific epitopes of the $GABA_A$-R subunit requires the immobilization of a ligand molecule in a solid support that should be easily concentrated and recovered after sedimentation.

Benzodiazepines (1,4-benzodiazepin-2-ones, BZDs) *i.e.* clonazepam (CNZ), diazepam (DZ), flunitrazepam (FNZ) (Scheme 1a) are drugs, pharmacologically grouped within the minor tranquillizers and widely used as anxiolytics, hypnotics and anticonvulsants. They stimulate inhibitory neurotransmission throughout the brain by enhancing the activity of the neurotransmitter γ-amino butyric acid (GABA). BZDs are not active *per se* but potentiate the GABA-mediated chloride conductances acting at a binding site located at $GABA_A$-R. The BZD binding site is different but allosterically related with the GABA binding site.[10]

In a previous work we reported the synthesis and characterization of an amphipathic CNZ (5-(2-hydroxyphenyl)-7-nitro-benzo[*e*][1,4]diazepine-2-(3*H*)-one) derivative capable of binding at the BZD site of the $GABA_A$-R through its hydrophilic end and to anchor in a biomembrane by means of its hydrophobic end, represented by a hydrocarbon chain attached at the N1 position.[11]

[a]*Biofísica-Química, Cátedra de Química Biológica, Departamento de Química, Facultad de Ciencias Exactas, Físicas y Naturales, Universidad Nacional de Córdoba, Av. Vélez Sarsfield 1611, 5016, Córdoba, Argentina. E-mail: mperillo@efn.uncor.edu; Fax: +54-351-4334139; Tel: +54-351-4344983 int 5*

[b]*INFIQC-Departamento de Química Orgánica, Facultad de Ciencias Químicas, Universidad Nacional de Córdoba. Av. Haya de la Torre s/n Ciudad Universitaria, X5000HUA, Córdoba, Argentina. E-mail: lauramoy@dqo.fcq.unc.edu.ar; Tel: 54-351-4334171 and 54-351-4334168*

† Electronic supplementary information (ESI) available: The ^{1}H-NMR and ^{13}C-NMR spectra and K *vs.* BDC molar fraction plot. See DOI: 10.1039/c1ob05210a

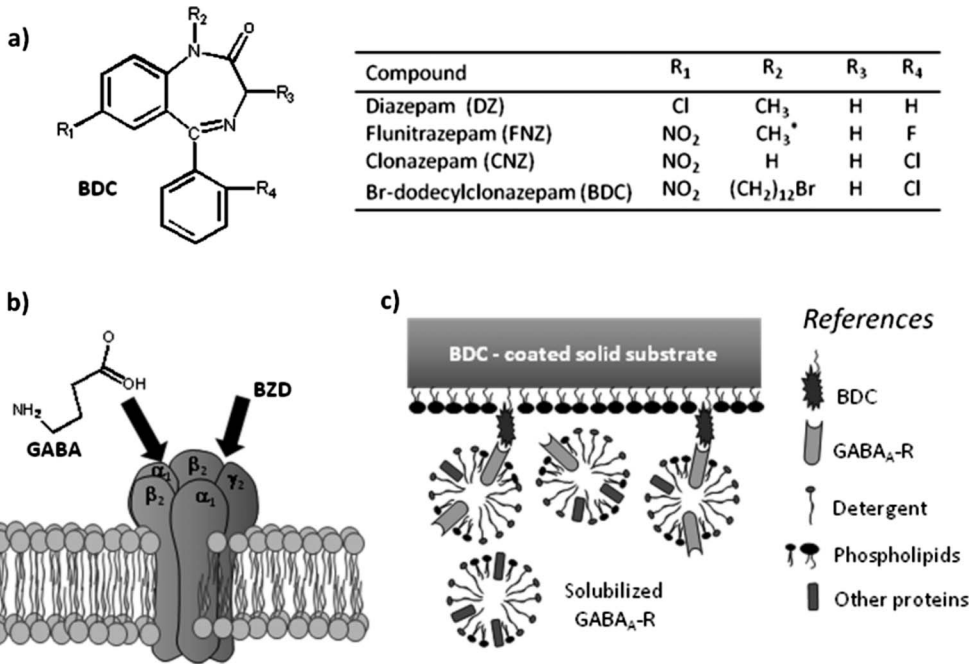

Compound	R_1	R_2	R_3	R_4
Diazepam (DZ)	Cl	CH_3	H	H
Flunitrazepam (FNZ)	NO_2	CH_3^*	H	F
Clonazepam (CNZ)	NO_2	H	H	Cl
Br-dodecylclonazepam (BDC)	NO_2	$(CH_2)_{12}Br$	H	Cl

Scheme 1 (a) General chemical structure and substituents of the BZDs used and synthesized in the present paper. • In [^{3}H]FNZ one of the H in R_2 is substituted by tritium. (b) Representation of the most abundant GABA$_A$-R isoform (subunit composition $\alpha_1\beta_2\gamma_2$)[37] inserted into SMs. The GABA$_A$-R is a pentamer composed of 5 subunits in a circular arrangement around a central axis. Each subunit contains a large extracellular N terminus, four α helix transmembrane domains, and a small extracellular C terminus. The N terminus forms a sandwich of β sheets, which bears the binding sites for GABA and BZDs.[37–39] In the scheme the ligand binding sites for GABA (between $\alpha_1\beta_2$ subunits) and for BZDs or BDC (between $\alpha_1\gamma_2$) are indicated. (c) Depiction of a solid substrate coated with a mixed phospholipid–BDC monomolecular layer binding purified GABA$_A$-R reconstituted in a micellar system. Coating may be achieved by the transference of the monolayers from the air–water interface to the solid substrate by the Langmuir–Blodgett technique.[33]

The design of this BZD derivative was based on theoretical studies on the BZD structure–activity relationship indicating that high affinity BZD analogues interacted with three GABA$_A$-R electrophilic groups located at C7, C2 and the iminic nitrogen N4. It is known that the N4 interaction is improved by the presence of halogens in C2′ and when the phenyl ring is rotated in the direction that confers greater coplanarity between the phenyl ring and the plane C1′–C5 = N4.[12] Consequently, some chemical modifications at the N1 position were not expected to affect (at least chemically) the BZD capacity to interact with the receptor binding site and our results confirmed this hypothesis.[11] So, the *N*1-octadecyl-CNZ was not only an active ligand at GABA$_A$-R but also was able to be spontaneously inserted in phospholipidic Langmuir films packed within a wide range of lateral surface pressures. Although it was partially excluded from the film at high molecular packings, in low proportions it could remain in the film up to the equilibrium surface pressures of natural membranes bilayers.

In spite of these promising results, the synthetic procedure applied gave rise to a methyl *N*-methylene glycinate as a secondary product; hence, to obtain the alkyl-CNZ with purity higher than 95%, the reaction mixture required a tedious purification procedure by TLC. Furthermore, a longer alkyl chain would confer on the CNZ derivative a longer surface for van der Waals dispersion interactions which would improve its membrane stability.

These previous findings motivated the development of a new and more effective synthetic procedure which was applied to the synthesis of a new CNZ derivative with a longer alkyl chain.

So, in the present paper we describe the synthesis, the GABA$_A$-R binding kinetics and biophysical properties of a 5-(2-hydroxyphenyl)-7-nitro-benzo[*e*][1,4]diazepin-2(*3H*)-one substituted at the N1 position with a dodecyl aliphatic chain containing a bromine atom at the end of the chain, which was denominated Bromo-dodecylclonazepam (BDC). The ability of this compound to interact and stabilize at the membrane–water interface was studied in monomolecular layers at the air–water interface by the Wilhelmy plate method. Molecular parameters determined from surface pressure–area isotherms were used to predict not only the type of self-assembled structures that BDC would be able to form in aqueous dispersions but also the molecular features that would contribute to enhancing the stability of this compound in the typical planar configuration that characterizes membrane bilayers. The presence of the bromine atom at the end of the alkyl chain provides this new derivative with the potential of interacting through halogen-bonding to appropriate electron donors. Hence, the possibility that this BDC may become surface-grafted and find several potential applications within the area of material science is discussed.

2. Experimental procedures

2.1 Materials

DZ and CNZ were kindly supplied by Products La Roche (Córdoba, Argentina). FNZ labeled with tritium (^{3}H) at the N1 position ([^{3}H]FNZ) was purchased from New England Nuclear Chemistry (E.I. DuPont de Nemours & Co. Inc., Boston, MA, USA). Dipalmitoylphosphatidylcholine was obtained from Avanti Polar Lipids (Alabaster, Al, USA). Other drugs and solvents were

Table 1 Experimental conditions of BDC (3) synthesis

Entry	Heating	Solvent	Base	*t* (min)	*T*/°C	% **3**
1	conventional	MeOH	NaOMe	1440	65	3
2	conventional	DMF	K_2CO_3	360	80	0
3	conventional	DMF	K_2CO_3	600	153	0
4	MW (CV)[a]	DMF	K_2CO_3	5.0	80	25
5	MW (CV)	DMF	K_2CO_3	7.5	80	40
6	MW (CV)	DMF	K_2CO_3	12.5	80	22
7	MW (CV)	DMF	K_2CO_3	22.5	80	0
8	MW (CV)	DMF	K_2CO_3	7.5	100	30
9	MW (CV)	—	K_2CO_3[c]	7.5	80	3
10	MW (OV)[b]	DMF	K_2CO_3	7.5	80	49
11	MW (OV)	—	K_2CO_3	7.5	80	11
12	MW (OV)	—	K_2CO_3[c]	7.5	80	2

[a] Closed-vessel conditions. [b] Open-vessel conditions. [c] Solvent free reactions: substrates were mixed with silica gel (100 mg **3**/100 mg silica).

of analytical grade. Merck silica gel 60 was used for filtration and Aldrich silica gel 60 F254 were used for preparative TLC. The chemical structures of the BZDs used are depicted in Scheme 1a.

2.2 NMR spectroscopy

All starting materials were commercially available and solvents were distilled and dried before use. ^{1}H and ^{13}C NMR spectra were recorded in a Bruker FT-400 (Rheinstetten, Germany) (^{1}H at 400 MHz and ^{13}C at 200 Hz) spectrometer using $CDCl_3$. Chemical shifts are reported in parts per million (ppm) downfield from TMS.

2.3 Procedure for preparation of CNZ derivative

In the first approach 0.2 mL of a methanolic solution of sodium methoxide (1.060 M) was added to a solution of CNZ (**1**) (0.152 mmol) in 25 mL of anhydrous methanol. The mixture was refluxed for a period of 15 min. After this time, 0.297 mmol of 1,12-dibromododecane (**2**) was added and subsequently refluxed for 24 h (Table 1, entry 1). After cooling, methanol was evaporated and the crude product was filtered using silica gel. This mixture was then purified by chromatographic column using hexane/ethyl acetate as eluents. Following this protocol, the desired 1-(12-bromododecyl)-5-(2-chlorophenyl)-7-nitro-1*H*-benzo[1,4]diazepin-2-one (**3**, BDC) was obtained with a very low yield (3%).

In the second methodology, 0.148 mmol of **1**, 0.222 mmol of **2** and 0.445 mmol of K_2CO_3 in 10 mL of anhydrous DMF were heated for 6 h in an oil bath at 80 °C (Table 1, entry 2) and for 10 h at 153 °C (Table 1, entry 3). Unfortunately, product **3** (or BDC) was never formed and a mixture of undesired products was obtained.

In the third methodology, 0.360 mmol of **1**, 0.538 mmol of **2** and 1.160 mmol of K_2CO_3, were dissolved in 3.3 mL of DMF. The mixture was subjected to microwave irradiation[13] in quartz closed-vessel and open-vessel systems for several minutes (5–22.5 min). A CEM Discover LabMate IntelliVent (USA, Matthews, North Carolina) reactor operating at 2.45 GHz with 300 W maximum power and thick-walled was used for MW irradiation. The runs were done in a temperature controlled mode and the irradiation power was set within the 40–300 W range. Temperatures were measured by means of an infrared sensor. In the case of closed-vessel experiments the pressure was set at 40 psi. The reaction mixture was then purified by chromatographic column using hexane/ethyl acetate as eluents to obtain the desired product. The highest yield obtained through this methodology (49%) was achieved after 7.5 min irradiation in an open-vessel system at 80 °C (see below and Table 1 for further explanation).

The characterization of compound **3** was done by ^{1}H NMR, ^{13}C NMR, HSQC, HMBC and COSY using $CDCl_3$ as solvent. Full spectra are provided as supporting information.†

5-(2-Chlorophenyl)-6-nitro-1-bromo-dodecyl-1,3-dihydro-2*H*-1, 4-benzodiazepin-2-one (**3**, **BDC**). ^{1}H NMR (400 MHz, $CDCl_3$), δ (ppm): 1.43 (m, 18H), 1.85 (q, J = 6.96 Hz, 2H), 3.41 (t, J = 6.88 Hz, 2H), 3.78 (m, 1H), 4.36 (m, 1H), 4.95 (d, J = 10.72 Hz, 1H), 3.81 (d, J = 10.72 Hz, 1H), 7.30 (m, 1H), 7.46 (m, 2H), 7.57 (d, J = 9.1 Hz, 1H), 7.66 (m, 1H), 7.94 (d, J = 2.64 Hz, 1H), 8.36 (d, J = 2.54 Hz y J = 9.08 Hz, 1H). ^{13}C (200 MHz, $CDCl_3$), δ (ppm): 26.91, 28.15, 28.44, 28.72, 29.16, 29.35, 29.41, 33.78, 47.49, 57.17, 122.57, 124.65, 126.00, 127.44, 130.38, 131.75, 132.97, 137.11, 139.20, 143.26, 147.10, 167.98, 168.52.

2.4 Monolayer studies

2.4.1 Surface pressure–area and surface potential–area compression isotherms. Monomolecular layers were prepared and monitored essentially as described previously.[14,15] Experiments were performed at room temperature. The surface pressure (π, Wilhelmy plate method *via* a platinized-Pt plate), surface potential (ΔV, vibrating plate method) and the area enclosing the monolayer (A) were automatically measured with a Minitrough II (KSV, Helsinki, Finland). The Teflon trough used had 24,075 mm^2 total area. Bidistilled water (230 mL total volume) was used as subphase. Lipid monolayers were formed by spreading, on the air–water interface, between 30–80 μL of a 2 : 1 chloroform–methanol solution containing 1 mg mL^{-1} of: a) the newly synthesized CNZ alkyl derivative (BDC), b) a pure saturated phospholipid (dipalmitoylphosphatidylcholine, dpPC) or c) a binary mixture dpPC–BDC at a molar fraction of BDC (x_{BDC}) varying between 0 and 1. The π–A and ΔV–A compression isotherms were recorded continuously, at a compression rate of 5 mm min^{-1}. The surface isotherm experiments were repeated at least twice.

2.4.2 Compressional modulus and critical packing parameter calculation. The compressional modulus (K) was calculated according to eqn (1).

$$K = -(A_\pi).\left(\frac{\delta\pi}{\delta A}\right)_\pi \quad (1)$$

The Critical Packing Parameter (P_c) was calculated according to the Israelachvili theory[16] by eqn (2).

$$P_c = \frac{v}{a_0 \cdot l_c} \quad (2)$$

The average molecular area (a_0) was experimentally determined from π–A isotherms, and optimal values for the hydrocarbon volume (v) and chain length (l_c) were calculated from eqn (3) and (4), according to Perillo *et al.*,[14] and refs. therein:

$$v \cong (27.4 + 26.9.n)n_{ch} \quad (3)$$

$$l_c \cong 1.5 + 1.265n \quad (4)$$

where n and n_{ch} are the number of methylene groups in the hydrocarbon chain and the number of chains per molecule, respectively. The molecular area (a_0) is a function of the interfacial free energy hence, it was assigned the actual mean molecular areas[17] at specific values of surface pressure taken from the π–A isotherm of each monolayer at the different compositions studied. P_c values for the binary dpPC–BDC mixtures were calculated from the weighted mean values of (v) and (l_c) of individual components.

2.4.3 Penetration of BDC in monomolecular layers of dpPC at the air–water interface. The aim of this experiment was to determine the maximum value of π that allowed drug penetration in the monolayer ($\pi_{cut\text{-}off}$). These experiments were done in a circular Teflon trough (4.5 cm diameter and 0.5 cm depth). Between 5 and 30 µL of a solution of dpPC in 2 : 1 chloroform : methanol were spread on an aqueous surface (bidistilled water) and about 5 min were allowed for solvents evaporation. Monolayers were prepared at constant surface area but at different initial surface pressures (π_i). The temporal variation of π induced by the BDC penetration into the monolayer after the injection of an ethanolic solution of the derivative in the subphase was measured until reaching a plateau (π_{max}). The values of $\Delta\pi = \pi_{max}$–π_i were plotted against π_i and a straight line was fitted to the experimental data. The $\pi_{cut\text{-}off}$ was determined from the intersection of the regression line with the abscissa axis.

2.5 Synaptosomal membrane preparations

Synaptosomal membranes (SM) were obtained from bovine cerebral brain cortex. Meninges were eliminated, the cortex dissected and the SM was purified essentially according to the method of Enna and Snyder, modified by Perillo and Arce,[18] lyophilized and stored at –20 °C. Immediately before used, membranes were resuspended in 50 mM pH 7.4 Tris–HCl buffer containing 100 mM NaCl at a final total protein concentration of 0.25 mg mL^{-1}. This SM suspension was used as membrane receptor preparation and $GABA_A$-R source in the experiments that followed.

2.6 Binding experiments

Binding was performed essentially as described previously.[19] The BZDs [^{3}H]FNZ and DZ were used as labeled and non-labeled ligands, respectively. Both compete for their reversible interaction with the same binding site at $GABA_A$-R (Scheme 1b). Due to their lipophilic characteristics, BZDs interact not only with the receptor (specific interaction) but also, through hydrophobic interactions, with the membrane as a whole by a partitioning process (non-specific interactions, NS) locating mainly at the polar head group region of the biomembranes.[20–23] Total binding (TB) and non-specific interactions (NB) are experimentally accessible but specific binding to the receptor (B) has to be calculated as a difference between TB and NB. The latter are irreversible. So, only the specific binding of [^{3}H]FNZ can be displaced from the receptor with high concentrations of a non-labeled ligand such as DZ and the remaining non-specifically bound [^{3}H]FNZ represents NS. TB is measured in the presence of the same concentration of [^{3}H]FNZ but in the absence of non-labeled ligand.

Thus, two sets of samples were prepared to measure the both NB and TB radiolabeled ligand bound to the membrane, respectively. The incubation system (230 µL final volume) contained: the SM suspension at a final total protein concentration of 0.25 mg mL^{-1} and 0.5–12 nM [^{3}H]FNZ (minimum specific activity 81.4 Ci mmol^{-1}). Then, 100 mM NaCl–50 mM Tris–HCl pH 7.4 buffer, containing (NB samples set) or not (TB samples set) 9.4 µM DZ were added.

Samples were incubated at 4 °C in the dark for 1 h and then filtered through SS filters Whatman GF/B type with a Brandel automatic filtration apparatus (Brandel, Gaithersburg, MD, USA). Then, filters were rinsed, dried in the air and placed in vials containing 2.5 mL of scintillation liquid (25% v/v Triton X-100, 0.3% w/v diphenyloxazole in toluene). The retained radioactivity was measured with a scintillation spectrometer Rackbeta 1214 (Pharmacia-LKB, Finland) at a 60% efficiency for tritium. Specific binding (B) was calculated as the difference between TB and NB determined in the absence and in the presence of DZ, respectively. Eqn (5) was fitted to the saturation curves (specific binding (B) *versus* free [^{3}H]FNZ concentration), by a non-linear regression analysis performed by a computer-aided least squares method:[17]

$$B = \frac{B_{max}.F}{K_d + F} \quad (5)$$

where F is the free [^{3}H]FNZ concentrations, B and B_{max} are the ligand concentration-dependent and the maximal specific binding activities, respectively, and K_d is the equilibrium dissociation constant. Protein concentration was determined by the method of Lowry.[24]

2.7 [^{3}H]FNZ displacement curve.

The aim of this experiment was to assess the ability of the newly synthesized BDC to displace [^{3}H]FNZ from its binding site at the $GABA_A$-R in SM. The experiments were carried out as described in Section 2.6 but using a constant concentration (2 nM) of radioligand ([^{3}H]FNZ) and in the presence of 0–50 µM BDC (final concentrations). The [^{3}H]FNZ concentration was chosen because of its equivalence with the thermodynamic dissociation constant (K_d) experimentally determined.

The IC_{50} values were determined from the % [^{3}H]FNZ bound *vs.* log BDC concentration (nM) plot, as the BDC concentration required to displace the 50% of [^{3}H]FNZ bound; K_i was calculated by means of the Cheng and Prusoff equation (eqn (6)),[17]

$$K_i = \frac{IC_{50}}{1 + \frac{[[^3H]FNZ]}{K_d}} \quad (6)$$

2.8 Critical micellar concentration determination

The critical micellar concentration (CMC) of BDC value was estimated as described previously.[25] Briefly, BDC was dispersed in water at different final concentrations (between 0 and 0.016 mM) in the presence or in the absence (Control) of the hydrophobic dye bromothymol blue (BTB) (80 μM final concentration). Samples were incubated at room temperature during 10 min and then the absorbance at 437 nm was measured with a Beckman DU 7500 (Fullerton, CA, USA) spectrophotometer. The absorbance values were plotted against the concentration of BDC (mM), and the CMC was estimated as the concentration of amphiphile at which the plot of absorbance *vs.* concentration suffered an abrupt slope change.

2.9 Statistical analysis

Binding data were statistically analyzed using a two-tailed Student's *t*-test for independent samples. $P < 0.05$ was considered as statistical significant. Regression analysis was done by the least squares method.[26]

3. Results and discussion

3.1 Synthesis of the probe precursor

The CNZ derivative (**3**, BDC) synthesis was performed using CNZ (**1**) as a $GABA_A$-R ligand and 1,12-dibromododecane (**2**) as hydrophobic rest under different conditions (Scheme 2 and Table 1). First, the reaction involved the formation of the sodium salt intermediate which then reacted with the dibromo derivative **2** in refluxing methanol to give the expected product in very low yields (3%). Several attempts to increase the formation of **3** were carried out however, the resulting yield could not be improved.

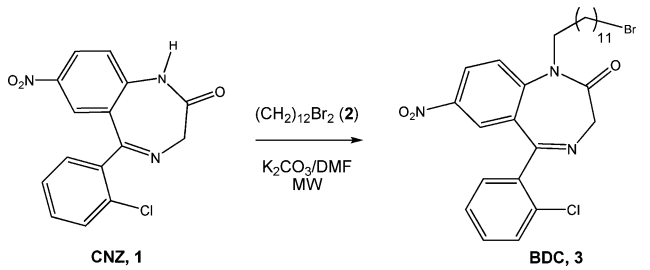

Scheme 2 Synthesis of BDC (**3**).

In view of the previous results, we decided to apply the methodology described in the regioselective aminoethylation of 1,4-benzodiazepinones.[27] Thus, we tried the *N*-alkylation of **1** using K_2CO_3 as a Brønsted–Lowry base and DMF as solvent at different temperatures and reaction times. Unfortunately, this change of reaction conditions did not lead to the expected product.

The use of microwave energy to heat chemical reactions has been shown to dramatically reduce reaction times, increase product yields and enhance product purities by reducing unwanted side reactions compared to conventional synthetic methods. For the advantages of the microwave chemistry, we applied this methodology to the *N*-alkylation of **1**. Thus, when a mixture of **1**, **2** and K_2CO_3 in DMF was irradiated at 80–100 °C in open- and closed-vessel systems, yields of **3** were notably increased up to 49% at 80 °C and irradiation time of 7.5 min (Table 1, entries 5 and 10). The increase of the reaction time at constant temperature, or *vice versa*, did not increase the amount of **3** probably because this compound decomposed under these severe conditions. Taking into account the advantages of carrying out the microwave transformations in dry media we decided to eliminate DMF from the reaction in an environmentally benign approach. Thus, solid reagents and base were mixed and subsequently irradiated. Analysis of the crude indicated the presence of mainly CNZ **1** (>90%) and traces of *N*-alkylated product (Table 1, entries 9, 11 and 12). This result could be explained by the reflection of penetrating microwaves by the reaction mixture in the absence of DMF and/or the inefficient stirring of the reagents during the irradiation process. When silica was used as inorganic support to improve the dispersion of active sites and facilitate the workup, conversion of **1** was poor (<5%) and a very small amount of product was obtained (Table 1, entries 9 and 12). On the other hand, it is known from the literature that there is a dependence of the yield of the products on the use of closed-vessel or open-vessel microwave heating. When we compared both types of microwave processing, the formation of **3** was slightly favored in open-vessel systems (Table 1, compare entries 5 and 10 or 9 and 12). Thus, *N*-alkylation of **1** requires the removal of the generated HBr to drive these reactions to completion and this process could be favored in open systems. Detailed spectra are provided as supporting information.†

3.2 [^{3}H]FNZ binding experiments

The aim of this experiment was to obtain the kinetic parameters necessary for the inhibition binding constant calculation (eqn (5)), as well as to evaluate the quality of the purified synaptosomal membranes as $GABA_A$-R source. B_{max} reflects the amount of $GABA_A$-R in SM and depends on the animal source (*i.e.* rat, monkey, chicken, and cow) and physiological state as well as the type of sub-cellular fractionation applied to obtain SMs. K_d is a measurement of the ligand–receptor binding affinity and from its value it would be possible to infer about the maintenance of the conformational stability of the receptor protein.

In these experiments, the specific binding of [^{3}H]FNZ was calculated from the total minus non-specific binding curves (Fig. 1, inset) as was described in the Materials and methods section. Fig. 1 shows a typical saturation curve. Eqn (4) was fitted to the experimental data and the kinetic parameters of the specific binding were determined as K_d = 2.27 ± 0.16 mM and B_{max} = 1715 ± 37 fmol x (mg protein)$^{-1}$. These values are in agreement with previous reports.[19]

3.3 [^{3}H]FNZ displacement experiments

The ability of BDC to displace [^{3}H]FNZ was evaluated by means of a radioligand competition assay. The results, depicted in Fig. 2, show that the 20–80% displacement of [^{3}H]FNZ specifically bound was achieved at BDC concentrations between 0.4 and 7.4 μM. However, BDC was unable to displace 100% of the total [^{3}H]FNZ

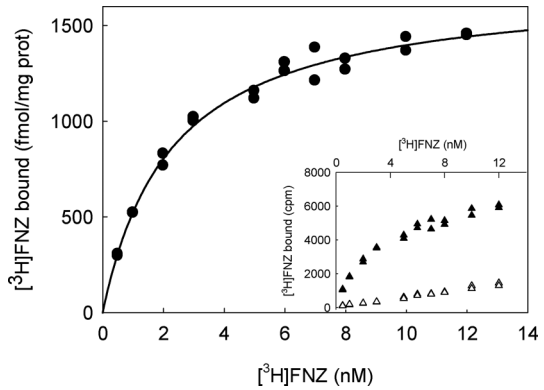

Fig. 1 Binding of [^{3}H]FNZ to synaptosomal membranes from bovine brain cortex. The DZ and protein concentration used were 9.24 μM and 0.25 mg protein mL^{-1}, respectively. (●) Specific binding. The inset shows the total (▲) and the non-specific (△) [^{3}H]FNZ binding curves.

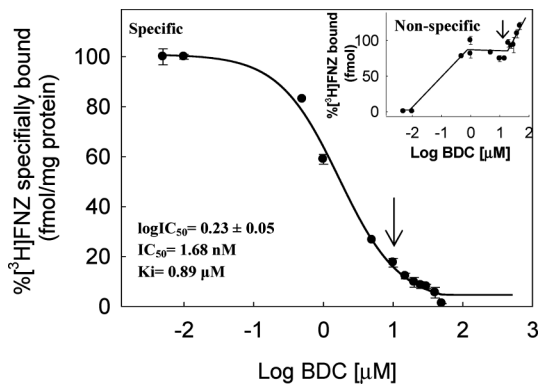

Fig. 2 BDC induced displacement of the [^{3}H]FNZ bound to synaptosomal membranes. The [^{3}H]FNZ and protein concentration used were 2 nM and 0.25 mg protein mL^{-1}, respectively. The inset shows the non-specific [^{3}H]FNZ binding. The arrow points to CMC_{BDC} value. Points above this concentration, where BDC is expected to be self-aggregated, were not considered for the fitting to eqn (6). Other details were described in the Experimental procedures section. Data shown are the mean ± s.e.m. of duplicates.

specifically bound to SM due to its self-aggregation. Assuming that BDC induces a competitive inhibition of [^{3}H]FNZ binding, a IC_{50} = 1.68 μM value was determined from data shown in Fig. 2 and the inhibition binding constant (K_i = 0.89 μM) of BDC was calculated from eqn (6). The non-specific [^{3}H]FNZ binding curve (inset in Fig. 2) showed a non-linear behavior indicating that some artefact was affecting the availability of ligand molecules to interact with SM, explaining the need for large amounts of BDC to displace [^{3}H]FNZ from its binding site in the $GABA_A$-R. Due to the relatively long alkyl chain, the BDC molecule has an amphipathic structure and the self-association of BDC molecules into micelles or other self-assembling structure could explain the non-specific curve shape. To investigate this hypothesis the critical micellar concentration of BDC (CMC_{BDC}) was determined.

3.4 BDC self-assembly

In order to confirm the self-assembling capability of BDC predicted from its molecular structure, the variation in the absorbance of BTB was evaluated as a function of the BDC concentration. The whole absorbance spectrum of BTB, which exhibited a maximum at 432 nm in water, suffered a red-shift (λ_{max} = 437 nm) as well as an hyperchromic concentration dependent effect in the presence of aromatic molecules such as terpenes.[25] The results, depicted in Fig. 3, showed that BDC induced an increase in BTB absorbance at 437 nm. The absorbance of BTB at 437 nm increases as a function of BDC concentration and at CMC_{BDC} it reached a maximum. This indicated the appearance of a new hydrophobic phase in the system compatible with the formation of self-assembled structures of BDC with an estimated CMC_{BDC} value of approximately 0.0105 mM. Note that the change in the slope of the non-specific binding curve occurs at a concentration equivalent to the CMC_{BDC}.

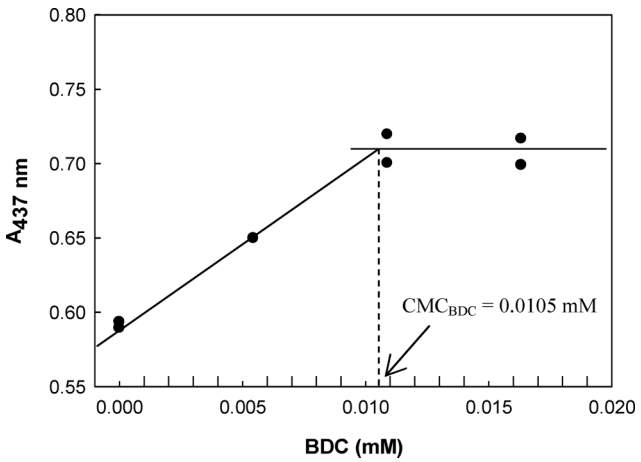

Fig. 3 BDC self-assembly in aqueous medium. Absorbance of BTB at 437 nm with respect to the control in water ($A_{437\,nm}$), as a function of the BDC concentration (mM). The CMC_{BDC} value (pointed to by the arrow) was estimated from the intersection of both regression lines.

3.5 Monomolecular layers at the air–water interface

3.5.1 Surface pressure–molecular area isotherms. Surface pressure–area isotherms are shown in Fig. 4. In Fig. 4a, an isotherm of pure dpPC is depicted as a reference. Dashed lines indicate the determination of the collapse pressure (π_c = 63.2 mN m^{-1}); the molecular area at the closest packing also known as minimal molecular area (Mma = 42.3 Å^2) and the transition surface pressure (π_T = 6 mN m^{-1}) corresponding to the liquid expanded/liquid condensed bidimensional phase transition characteristic of dpPC.

BDC was able to form monomolecular layers at the air–water interface both alone (Fig. 4a) as well as in mixtures with dpPC at various molar fractions (x) (Fig. 4b). From the analysis of the π–A compression isotherm of BDC (Fig. 4a), a collapse pressure π_c = 9.8 mN m^{-1} and Mma = 52 Å^2 were determined and no bidimensional transitions were observed. If compared with dpPC, BDC monolayer exhibited a lower stability as reflected by its lower π_c value which may be due to the shorter length of its hydrocarbon chain that provides a low London dispersion energy stabilizing the aggregate which, at high π near π_c, is not enough to counterbalance the repulsive interactions between the polar head groups. This leads to an inefficient molecular packing explaining the fact that, in spite of having only one hydrocarbon chain and not two as in

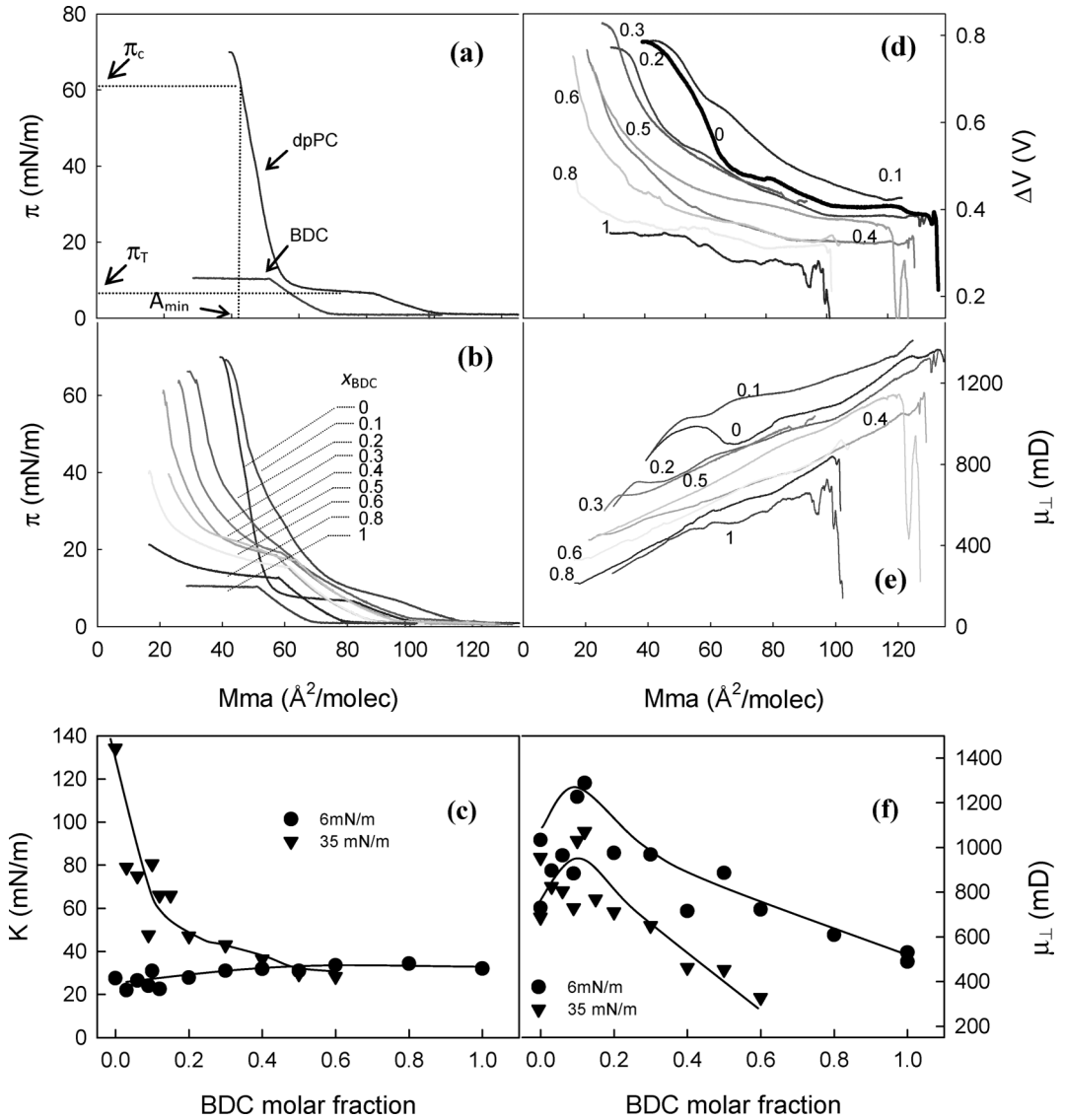

Fig. 4 Behavior of dpPC/BDC binary mixtures at the air–water interface. a) π–Mma compression isotherms of pure dpPC and pure BDC. Collapse pressure (π_c), transition pressure (π_T) and minimal molecular area (A_{min}) determination exemplified over a dpPC π–A compression isotherm. b) Surface pressure–Mma isotherms of dpPC–BDC binary mixtures. c) Compressional modulus at 6 and 35 mN m^{-1}, as a function of monolayer composition. d) Surface potential–Mma and e) $\mu_\perp$–Mma compression isotherms of dpPC–BDC binary mixtures. Dipole moments ($\mu_\perp$) were calculated according to eqn (6) from ΔV values taken from panel (d) and were plotted as a function of Mma. f) Resultant dipole moment at 6 (●) and 35 (▼) mN m^{-1}, as a function of monolayer composition. Small numbers in panels b, d and e refer to x_{BDC}.

the case of dpPC, BDC exhibits a minimal molecular area higher than that of the phospholipid.

The BDC–dpPC mixtures exhibited full miscibility up to $x_{BDC} \cong 0.1$ (Fig. 4b). Above $x_{BDC} = 0.1$, mixtures showed composition-dependent surface pressure transitions (not related with the bidimensional surface pressure of dpPC, which occurs at a lower π). Upon further compression these monolayers collapse at a composition-independent $\pi \cong \pi_c$ of pure dpPC (Fig. 5), suggesting that those transitions may consist of a partial collapse of the monolayer. This also suggested a partial miscibility of both components. Further analysis was done through a phase diagram (Fig. 5).

The effect of the proportion of BDC in the mixtures with dpPC on the elasticity of monolayers was analyzed through the compressibility modulus K (Fig. 4c) in conditions of full miscibility at all compositions (6 mN m^{-1}) or of compositionally-dependent miscibility (35 mN m^{-1}). At 6 mN m^{-1}, K exhibited a tendency to increase continuously as a function of x_{BDC} up to $x_{BDC} = 0.6$ reflecting both the higher coherence of BDC films with respect to the liquid expanded phase of dpPC (corresponding to $x_{BDC} = 0$) as well as full miscibility of both compounds at this lateral pressure. Above $x_{BDC} = 0.6$, K values did not change and the curve reached a *plateau*. At 35 mN m^{-1}, K decreased abruptly as a function of x_{BDC} up to $x_{BDC} \cong 0.1$ and at higher x_{BDC} showed a dispersion in the data set around the line drawn to follow the eye that reinforced the different miscibility regimes exhibited by the phase diagram (the miscibility of BDC in dpPC is partially lost at $x_{BDC} \geq 0.1$).

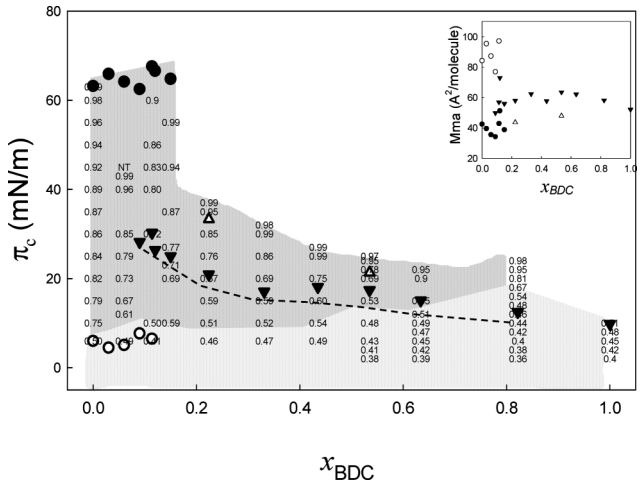

Fig. 5 Surface pressure–composition phase diagram overlapped with critical packing parameter (P_c) for dpPC–BDC mixtures. The phase diagram (π–x_{BDC}) was constructed using π_c values (●), typical pure dpPC bidimensional phase transition pressures (○) and the phase transitions pressures (△) or partial collapse pressures (▼), identified as slope changes in Fig. 4b detected trough minima in the *K vs.* Mma plot. Numbers on the graph refer to P_c values calculated for each mixture at the specified surface pressure. Note that above the line joining the phase transition points (▼) (at $x_{BDC} > 0.1$) P_c values would be meaningless due to immiscibility. Predicted type of self-assembled structures formed were indicated by the dark shadowed area with $0.5 < P_c < 1$ in the case of bilayers and a light shadowed area with $P_c \leq 0.5$, for micelles. The inset shows the Mma corresponding to those surface pressures at which bidimensional phase transitions and collapses occur, at each of the x_{BDC} studied. (■) Mma at the monolayer collapse point (▼ and △) other bi-dimensional phase transitions observed in mixtures.

3.5.2 Surface electrostatics. The surface potential ΔV–area isotherms (Fig. 4d) showed that ΔV increased upon compression and decreased as a function of BDC in the mixtures. At the closest packing ΔV_{dpPC} = 750 mV and ΔV_{BDC} = 340 mV while the mixtures showed intermediate values. Although the ΔV–area isotherm for dpPC showed in Fig. 4 exhibits higher ΔV values compared to most reports that have appeared lately,[28–30] its shape as well the shape and π values of the π–area isotherm measured simultaneously in the same monolayer are correct. Hence, on a relative basis, the effect of BDC on the electrostatics of its binary mixtures with dpPC is reliable.

Surface potential is a measure of the electrostatic field gradient perpendicular to the membrane interface and thus varies considerably with the molecular surface density and with changes in orientation accompanying the monolayer compression. Taking the dielectric constant of the medium as unity, the molecular dipole moment can be calculated according to eqn (7):

$$\Delta V = 12.\frac{\pi}{A}\mu_{\perp} + \psi_0 \qquad (7)$$

where π = 3.1416, A (molecular area) and V (surface potential) are expressed in Å^2.molecule^{-1} and mV, respectively, $\mu_{\perp}$ (expressed in debye units, mD) is the apparent (resultant) perpendicular dipole moment of the molecule and ψ_0 is the electrostatic potential difference at the interface with respect to bulk subphase solution in ionized monolayers and modified by the ionic double layer (for uncharged molecules $\psi_0 = 0$).[14,15] The parameter $\mu_{\perp}$ contains different electrostatic contributions. In the case of uncharged molecules such as dpPC (a zwitterionic phospholipid), and BDC (uncharged at the pH assayed) the main contribution arises from the resultant dipole moments of the monolayer components and those of the water hydration network (water molecules oriented at the polar headgroup). In turn, contributions from monolayer components include the polar headgroup and hydrocarbon chains contributions. A general decrease in the magnitude of $\mu_{\perp}$ was observed upon compression due to molecular reorientations at the surface (Fig. 4e). While the whole plot of $\mu_{\perp}$ *vs.* Mma at x_{BDC} = 0.1 was above that of the pure dpPC, it was observed a decreasing trend in $\mu_{\perp}$ *vs.* Mma plots up on increasing x_{BDC}. In conjunction with the information taken from the π–Mma curves, this can be interpreted as an indication of a monolayer compositional change as a consequence of its destabilization at high surface pressures. Fig. 4f shows that, after an initial increase of $\mu_{\perp}$, within the π range exhibiting total mixing between dpPC and BDC, $\mu_{\perp}$ decreased as a function of x_{BDC}. At high surface pressure (35 mN m^{-1}), $\mu_{\perp}$ values were lower than those at 6 mN m^{-1}, with a decreasing tendency at $x_{BDC} > 0.1$ even more noticeable than at 35 mN m^{-1}.

3.5.3 Phase diagrams of dpPC–BDC binary mixtures and prediction of their self-assembling structures in water. From minimal values observed in K–Mma curves (see supporting information†), the π–x phase diagrams were constructed (Fig. 5). Lines in Fig. 5 indicate the presence of π–x states at which phase transitions occur and delimit regions of a single bidimensional phase that may coexist with an already collapsed phase.

A single monolayer phase can be found at low pressures within the whole compositional range. This monolayer shows a π_T similar to that of the pure dpPC up to $x_{BDC} \cong 0.1$ (hollow circles) which can be associated with a bidimensional phase transition, and collapses at $\pi_c \cong 63$ mN m^{-1} (pure dpPC). At $x_{BDC} \geq 0.1$ a partial collapse of the monolayer occurs (hollow circles). This is supported by the inspection of the π–A isotherm shape at x_{BDC} = 0.1 which shows that the x_{BDC}-dependent collapse point decreases up to the point where π_c equaled the π_c value of pure BDC. At higher pressures a second collapse point is observed (x_{BDC} = 0.1 and 0.3) with a composition-dependent π, probably consisting of a remaining dpPC–BDC mixture stable at the air–water interface.

Finally, at $x_{BDC} < 0.1$ π_c increases (black circles), then BDC seems totally miscible in dpPC exhibiting a bidimensional phase transition between 5–8 mN m^{-1}.

Critical packing parameter values (P_c) allow the prediction of the type of self-assembling structures that would be form when an amphipathic substance is dispersed in water. P_c values for the binary dpPC-BDC mixtures were calculated by eqn (2)–(4) using Mma values taken from the isotherms shown in Fig. 4b. These P_c values were superimposed on the phase diagram (Fig. 5). $P_c < 0.5$ predicts the self-assembling into micelles, $0.5 < P_c < 1$ predicts the self-association into bilayer phases which would lead to the formation of vesicles. $P_c > 1$ would correspond to phases with negative curvature and although they are not predicted in Israelachvili's theory, they are compatible with inverted vesicles, such as with hexagonal II or cubic phases.[14,31] According to this interpretation given to data in Fig. 5, within the region located at the left side of the π–x_{BDC} phase space (at low x_{BDC} (<0.1) and at all π above π_T), the resulting P_c values were compatible with the formation of bilayers. At the bottom within the whole

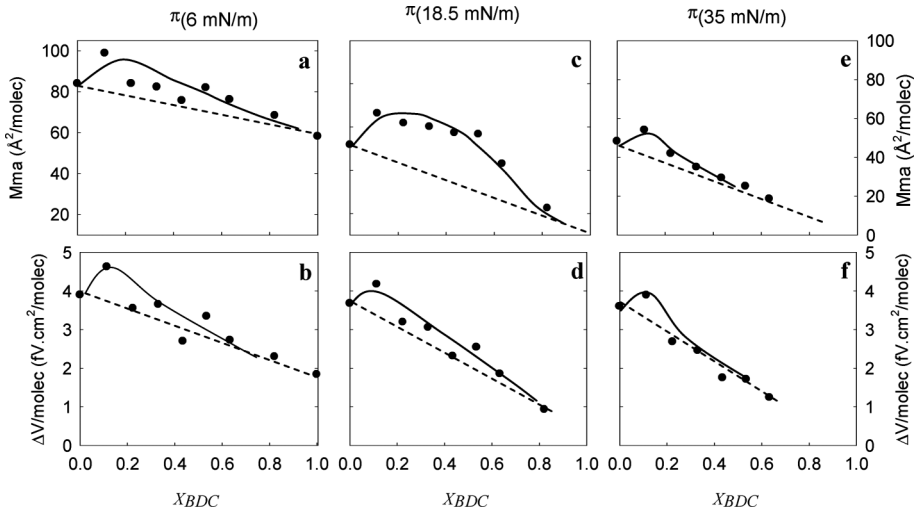

Fig. 6 Mean molecular area (a, c and e) and surface potential per unit of molecular surface density (b, d and f) *vs.* composition plots at constant surface pressures. Mma values (a, c and e) and ΔV/molec (b, d and f) values at different molar fractions of BDC and at constant $\pi = 6$ (a,b), 18.5 (c,d) or 35 mN m^{-1} (e,f). Dashed lines represent the behavior expected for ideal mixing or complete segregation of the components. Deviations from this behavior are more clearly reflected in Mma–x plots.

range of x_{BDC}, P_c values predicted the formation of micelles (light shadowed area) or bilayers (dark shadowed area). The region above the line joining the black triangles had P_c values which, although compatible with a bilayer ($P_c > 0.5$), should be considered meaningless due to the partial collapse. Hence, to obtain stable planar membranes at a π compatible with the equilibrium surface pressure of biomembranes (near 30–35 mN m^{-1}) the molar faction of BDC should not exceed 0.1.

The analysis of the variation of the Mma (mean molecular area) or the ΔV/molec (surface potential per unit of molecular surface density) with the mole fraction (x_{BDC}) at constant packing conditions ($\pi = 6$, 18.5 and 35 mN m^{-1}) is shown in Fig. 6. Straight dotted lines joined the values corresponding to the molecular parameters of pure dpPC and pure BDC. Experimental points lying on this line would represent states with either an ideal mixing or immiscibility behavior of components in the monolayer. The compositional dependence or independence, respectively, of the collapse pressure might help to discriminate between both behaviors. Mma (Fig. 6a, 6c, 6e) as well as ΔV/molec (Fig. 6b, 6d, 6f) decreased as a function of x_{BDC}. At 6 mN m^{-1}, Mma showed positive deviations from ideality, suggesting repulsive interactions or other steric restrictions to the ideal molecular packing between the monolayer components. Deviations from ideality in Mma and those in ΔV/molec were small or negligible, respectively. These results indicate that the permanence of BDC at high proportions in the monolayer at low π disrupts the lateral organization of the phospholipids (Mma is expanded) without affecting significantly the coherence of the molecular orientation in the monolayer (small changes in ΔV/molec). At 18.5 and 35 mN m^{-1}, Mma and ΔV/molec *vs.* x_{BDC} plots decreased discontinuously up to the abscissa axis and reached the zero value. The behavior in the Mma–x_{BDC} plot at 18.5 mN m^{-1} was similar to that at 6 mN m^{-1}. This surface pressure (18.5 mN m^{-1}) was still within the miscibility region up to $x_{BDC} = 0.6$ according to the phase diagram. Strong positive deviation from ideality was observed in Mma (Fig. 6c) while ΔV exhibited a negligible positive deviation (Fig. 6d). At 35 mN m^{-1} the monolayer phase exists up to $x_{BDC} \cong 0.6$ and at higher proportions of BDC a discontinuity was shown in Mma plot (there is no data at these π and x_{BDC}, as shown in Fig. 4b and 5). Negligible expansion was observed with respect to the ideality in Mma (Fig. 6e) and in ΔV x molec^{-1} (Fig. 6f) only at $x_{BDC} \leq 0.2$.

3.5.4 BDC penetration in phospholipids monolayers. The ability of BDC to penetrate in monomolecular layers of dpPC from the aqueous subphase was evidenced by the π increase at constant area at different initial surface pressures up to a $\pi_{cut\text{-}off} = 34.8 \pm 0.8$ mN m^{-1}. This value was determined by extrapolating the plot of $\Delta\pi$ *versus* π_i to $\Delta\pi = 0$ (Fig. 7). On the other hand, the smooth variation of the monolayer compressibility (K) with x_{BDC} also showed that BDC was stable in the film at low molecular packings (low π). Above 34.8 mN m^{-1} BDC did not penetrate in the film from the subphase ($\Delta\pi = 0$) while K at high π (Fig. 4c) suffered a discontinuous variation with x_{BDC} at $x_{BDC} > 0.2$, and at $x_{BDC} > 0.3$ the BDC–dpPC mixture partially collapsed at $\pi \leq 20$ mN m^{-1} (Fig. 5). Taken together these results suggested that it was possible to stabilize small amounts of BDC in highly packed monolayers (at lateral surface pressures compatible with the equilibrium pressure of bilayers – *ca.* 30–35 mN m^{-1}, ref. 32), independently of the direction from which the drug accessed the model membrane.

In general terms, the drug access from the aqueous phase to the membrane can be considered as part of a partition process and a kind of non-specific interaction. Thus, the results presented in this section suggest the possibility of using BDC as a precursor to develop a molecular probe to allow the evaluation of the molecular organization of SM within the molecular surroundings of $GABA_A$-R. Similar to what was proposed for OC,[11] the probe would partition in the membrane with a preferential binding to the receptor through the CNZ moiety and then to the membrane though the hydrocarbon tail. For this it will be required to modify BDC by the covalent attachment of an environmentally sensitive

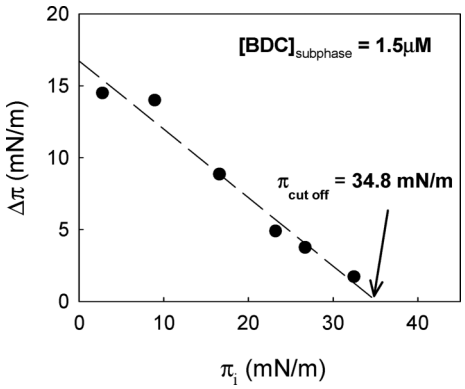

Fig. 7 BDC penetration in monomolecular layers of dpPC at different initial molecular packings. The line represents the fit of a straight line to the experimental points by regression analysis by the least squares method. The $\pi_{cut\text{-}off}$ value, indicated by the arrow, represents the maximal π allowing the drug penetration and monolayer deformation. Regression line is defined by the equation: $\Delta\pi = a + b\pi_i$, where a is the ordinate (16.7 ± 0.8 mN m^{-1}) and b the slope (–0.48 ± 0.04 mN m^{-1}). At $\Delta\pi = 0$, π_i equals the $\pi_{cut\text{-}off}$ = 34.8 mN m^{-1}.

label (fluorescent or paramagnetic) in its molecular structure, preferably at the hydrocarbon chain.

On the other hand, the objective, as proposed in the present paper, of immobilizing BDC at the surface of microparticles should be accomplished in a two-step procedure. BDC molecules will be firstly incorporated in a monomolecular layer at the air–water interface (1st step) which will be subsequently transferred to a solid substrate by the Langmuir–Blodgett technique (2nd step).[33] In this case London-type dispersion interaction between BDC and phospholipid hydrocarbon chains (which can be considered a kind of non-specific interaction) would contribute to the stabilization of BDC at the film and will reduce its exchange (partitioning) between Langmuir–Blodgett films and the nanoparticles containing the solubilized $GABA_A$-R (Scheme 1c).

4. Conclusions

In the present paper we described the synthesis, the biophysical characterization and the $GABA_A$-R binding kinetics properties of a new clonazepam derivative (BDC).

The goal of this work was the use of microwave radiation as a non-conventional energy source showing better selectivity towards the desired product. This methodology increased the yield of the desired product (BDC) in very short reaction times and facilitated the product purification.

In a previous work, we obtained a clonazepam derivative bearing an 8 carbon alkyl chain attached al N1 position (octyl clonazepam, OC). This molecule was able to interact with the $GABA_A$-R and stabilize at the membrane–water interface but with a π_{cutoff} = 13 ± 5 mN m^{-1}. Above 13 mN m^{-1}, OC not only did not penetrate in the film from the subphase, but also from the π–Mma isotherm analysis and the phase diagram, K at high π suffered a discontinuous variation with x_{OC} at $x_{OC} > 0.2$, suggesting that it was not possible to stabilize high amounts of OC in highly packed monolayers independently of the direction from which the drug reached the model membrane. The new derivative BDC, was less stable at the air–water interface (lower π_c) than OC probably due to packing defects introduced by the bromine atom at the methyl end but improved its ability to penetrate into dpPC monolayers showing a $\pi_{cut\text{-}off}$ = 34.8 ± 0.8 mN m^{-1}, even at a lateral surface pressure compatible with the equilibrium pressure of bilayers.

Table 2 Physico-chemical characteristics of OC and BDC derivatives as compared with dpPC all at the closest packing

Property (units)	dpPC	OC	BDC
alkyl chain length	16	8	12
π_c (mN m^{-1})	63	18.8	9.8
Mma (Å^2/molec)	42	49	52
$\Delta V_{\pi c}$ (V)	0.750	0.296	0.340
$\mu_{\perp,\pi c}$ (mD)[a]	835	385	462
K_c (mN m^{-1})	213	55	31.2
P_c[b]	0.75	0.35	0.51
Predicted self-assembling structure[c]	bilayer	micelle	micelle
x_{max} for 0.5 < P_c < 1 at π = 30 mN m^{-1}[d]	—	0.3	0.1
$\pi_{cut\text{-}off}$ (mN m^{-1})	—	13	34.8
K_i (nM)	—	176	890

[a] Calculated as indicated in Section 2.4.2. [b] Calculated at π_c of BDC. [c] Type of structure of self-assembling formed upon dispersed in water. [d] Highest molar fraction allowing self-assembly into bilayers at a surface pressure of 30 mN m^{-1}.

On the other hand, the calculated inhibition binding constant of BDC was K_i = 0.89 μM, indicating a very low affinity of BDC to the benzodiazepines binding site in the $GABA_A$-R. The marked amphipathic structure of the BDC molecule dictated its tendency to self-association in aqueous media with a CMC_{BDC} = 0.0105 mM and could explain the shape of the non-specific binding curve as well as the large amount of BDC necessary to displace [^{3}H]FNZ from the $GABA_A$-R. The main physico-chemical characteristics of both OC and BDC derivatives are shown in Table 2.

This finding may contribute to the use of BDC as a probe to evaluate the molecular organization of SM in the molecular surroundings of $GABA_A$-R, similar to the OC molecule. In addition, in spite of the relatively low affinity exhibited by BDC dispersed in water it would be an interesting tool to develop a binding-based precipitation method to purify $GABA_A$-R based on BDC coated microparticles (Scheme 1c). This system may be proposed as a useful succedaneum of traditional immunoprecipitation procedures to avoid the requirement of monoclonal antibodies against specific epitopes of $GABA_A$-R subunits.[34] The method of preparation of the ligand-coated particle would be fast, the particle would be recoverable, permitting repeated micro or large scale one-step purification of $GABA_A$-R without antibody requirements. Under those conditions, with the alkyl chain immobilized at a solid substrate, the self-aggregation of BDC into micelles or other highly curved structured would be prevented and the specific binding interaction of the CZ moiety to the BZD site in the $GABA_A$-R would be improved. Considering our results, the microparticles of alkylated glass could be coated with a monomolecular layer of a dpPC–BDC mixture $x_{BDC} \leq 0.1$ to ensure the homogeneous distribution of BDC molecules on the particle surface and free access of BDC to the receptor site. Furthermore, advantage can be taken of the presence of a Br atom at the methyl end of BDC to stabilize this compound to a surface of appropriate chemical composition through halogen bonding interactions.

Halogen bonding is the non-covalent interaction between halogen atoms (Lewis acids) and neutral or anionic Lewis bases. There is a close similarity with hydrogen bonding. Although halogen-bonding interactions such as the iodine–oxygen interaction were known in the early 1950s, the study of the halogen bond and its application in supramolecular chemistry, crystal engineering, and materials science has resumed in recent years.[35,36] This would further enable us to design and manipulate novel halogen-bonded functional supramolecular materials based on BDC that might allow useful applications beyond our immediate interest in the $GABA_A$-R purification system.

Abbreviations

BDC	bromo-dodecylclonazepam
BZD	benzodiazepines
CMC	critical micellar concentration
CNZ	clonazepam
COSY	Correlation Spectroscopy H^1–H^1
DMF	dimethylformamide
dpPC	dipalmitoylphosphatidylcholine
DZ	diazepam
FNZ	flunitrazepam
GABA	gamma aminobutyric acid
$GABA_A$-R	$GABA_A$ receptor
HSQC	Heteronuclear Single Quantum Correlation
HMBC	Heteronuclear Multiple Bond Correlation
NMR	nuclear magnetic resonance spectroscopy
NOE	Nuclear Overhauser Effect
OC	octadecylclonazepam
SEM	standard error of the mean
SM	synaptosomal membranes
TLC	thin layer chromatography

Acknowledgements

The present work was partially financed by grants from CONICET, SECyT-Universidad Nacional de Córdoba and ANPCyT from Argentina. B.C. is a Ph.D. student of the Doctorado en Ciencias Biológicas of the Universidad Nacional de Córdoba. G.J.Q. is a Ph.D. student of the Doctorado en Ciencias Químicas of the Universidad Nacional de Córdoba. G.J.Q. and B.C. are fellowship holders and. A.V.T, E.L.M, and M.A.P are Career Investigators from CONICET.

References

1 R. Sogaard, T. M. Werge, C. Bertelsen, C. Lundbye, K. L. Madsen, C. H. Nielsen and J. A. Lundbaek, *Biochemistry*, 2006, **45**, 13118–13129.
2 J. A. Lundbaek, P. Birn, A. J. Hansen, R. Sogaard, C. Nielsen, J. Girshman, M. J. Bruno, S. E. Tape, J. Egebjerg, D. V. Greathouse, G. L. Mattice, R. E. Koeppe, 2nd and O. S. Andersen, *J. Gen. Physiol.*, 2004, **123**, 599–621.
3 D. A. Kelkar and A. Chattopadhyay, *Biochim. Biophys. Acta, Biomembr.*, 2007, **1768**, 1103–1113.
4 M. O. Jensen and O. G. Mouritsen, *Biochim. Biophys. Acta, Biomembr.*, 2004, **1666**, 205–226.
5 A. G. Lee, *Biochim. Biophys. Acta, Biomembr.*, 2004, **1666**, 62–87.
6 A. Pallandre, B. de Lambert, R. Attia, A. M. Jonas and J. L. Viovy, *Electrophoresis*, 2006, **27**, 584–610.
7 W. Sieghart, *Trends Pharmacol. Sci.*, 1992, **13**, 446–450.
8 S. M. Dunn and R. P. Thuynsma, *Biochemistry*, 1994, **33**, 755–763.
9 K. Kannenberg, R. Baur and E. Sigel, *J. Neurochem.*, 1997, **68**, 1352–1360.
10 A. K. Mehta and M. K. Ticku, *Brain Res. Rev.*, 1999, **29**, 196–217.
11 A. V. Turina, B. Caruso, G. I. Yranzo, E. L. Moyano and M. A. Perillo, *Bioconjugate Chem.*, 2008, **19**, 1888–1895.
12 G. H. Loew, J. R. Nienow and M. Poulsen, *Mol. Pharmacol.*, 1984, **26**, 19–34.
13 A. Bangham, M. Hill and N. Miller, *Methods in Membrane Biology*, ed. E. D. Korn, Plenum Press, New York, 1974.
14 M. A. Perillo, A. Polo, A. Guidotti, E. Costa and B. Maggio, *Chem. Phys. Lipids*, 1993, **65**, 225–238.
15 G. Gaines, *Insoluble Monolayers at Liquids-Gas Interfaces*, Interscience Publishers, New York, 1966.
16 J. N. Israelachvili, *Intermolecular and Surface Forces*, Academic Press, New York, 1989.
17 H. I. Yammamura, S. J. Enna and J. K. Michael, *Neurotransmiter Receptor Binding*, Raven, New York, 1978.
18 M. A. Perillo and A. Arce, *J. Neurosci. Methods*, 1991, **36**, 203–208.
19 M. A. Perillo, D. A. Garcia, R. H. Marin and J. A. Zygadlo, *Mol. Membr. Biol.*, 1999, **16**, 189–194.
20 M. A. Perillo, D. A. Garcia and A. Arce, *Mol. Membr. Biol.*, 1995, **12**, 217–224.
21 D. A. Garcia and M. A. Perillo, *Biomed. Chromatogr.*, 1997, **11**, 343–347.
22 D. A. Garcia and M. A. Perillo, *Biochim. Biophys. Acta, Biomembr.*, 1999, **1418**, 221–231.
23 D. A. Garcia and M. A. Perillo, *Biophys. Chem.*, 2002, **95**, 157–164.
24 O. H. Lowry, N. J. Rosebrough, A. L. Farr and R. J. Randall, *J. Biol. Chem.*, 1951, **193**, 265–275.
25 A. V. Turina, M. V. Nolan, J. A. Zygadlo and M. A. Perillo, *Biophys. Chem.*, 2006, **122**, 101–113.
26 R. Sokal and F. Rohlf, *Introduction to Biostatistics*, W. H. Freeman & Company, New York, 1987.
27 J. K. Mishra, J. Srinivasa Rao, G. Narahari Sastry and G. Panda, *Tetrahedron Lett.*, 2006, **47**, 3357–3360.
28 M. Winterhalter, H. Burner, S. Marzinka, R. Benz and J. J. Kasianowicz, *Biophys. J.*, 1995, **69**, 1372–1381.
29 V. L. Shapovalov, *Thin Solid Films*, 1998, **327-329**, 599–602.
30 K. Sabatini, J. P. Mattila, F. M. Megli and P. K. Kinnunen, *Biophys. J.*, 2006, **90**, 4488–4499.
31 M. A. Perillo, N. J. Scarsdale, R. K. Yu and B. Maggio, *Proc. Natl. Acad. Sci. U. S. A.*, 1994, **91**, 10019–10023.
32 D. Marsh, *Biochim. Biophys. Acta*, 1996, **1286**, 183–223.
33 E. M. Clop, P. D. Clop, J. M. Sanchez and M. A. Perillo, *Langmuir*, 2008, **24**, 10950–10960.
34 M. J. Duggan, S. Pollard and F. A. Stephenson, *J. Biol. Chem.*, 1991, **266**, 24778–24784.
35 P. Metrangolo, H. Neukirch, T. Pilati and G. Resnati, *Acc. Chem. Res.*, 2005, **38**, 386–395.
36 J. Xu, X. Liu, J. Kok-Peng Ng, T. Lin and C. He, *J. Mater. Chem.*, 2006, **16**, 3540–3545.
37 S. W. Baumann, R. Baur and E. Sigel, *J. Biol. Chem.*, 2001, **276**, 36275–36280.
38 Y. Muroi, C. Czajkowski and M. B. Jackson, *Biochemistry*, 2006, **45**, 7013–7022.
39 J. E. Baenziger and P. J. Corringer, *Neuropharmacology*, 2011, **60**, 116–125.